

<https://doi.org/10.1038/s43247-025-02646-x>

Unraveling the seasonality of functional diversity through remote sensing



Daniel Mederer ¹ ✉, Teja Kattenborn ², Eya Cherif ^{1,3}, Claudia Guimaraes-Steinicke¹,
Julia S. Joswig ¹, Fabian D. Schneider ^{4,5} & Hannes Feilhauer ^{1,3,6,7}

Plant functional diversity is a key biodiversity indicator of ecosystem dynamics. Several studies have shown that spectral data from Earth observation satellites will enable us to map functional diversity over large areas. However, most studies only consider snapshots of such data in time, and our knowledge of the temporal variation of functional diversity across the World's biomes remains sparse. Here, we use hyperspectral remote sensing and deep learning to explore multi-seasonal functional diversity patterns on a global scale. We show that functional diversity can be highly dynamic over time. These dynamics are biome-specific, driven by seasonal cycles and wet-dry periods. Our findings highlight that the role of functional diversity in shaping ecosystem dynamics can be unraveled only by incorporating seasonality into functional diversity mapping. Such a multi-temporal approach will enhance the robustness of functional diversity assessments and deepen our understanding of ecosystem responses to environmental change.

Biodiversity of plants encompasses various facets, including species diversity, structural diversity, functional diversity, and genetic diversity, all of which are increasingly threatened by the ongoing global biodiversity crisis¹. Among these, the loss of plant functional diversity—the variety of plant functional traits within a community or an ecosystem—poses significant risks to ecosystem productivity², functioning, and stability^{3–6}. In this context, plant functional traits are valuable indicators of ecosystem processes and reliable proxies for assessing ecosystem conditions^{7,8}. Thus, monitoring of functional diversity is crucial for a deeper understanding of ecosystem dynamics. Ideally, such monitoring should occur continuously and extend globally. However, measuring functional diversity requires assessing variations in multidimensional trait space^{9–13}, and obtaining such plant trait data at the community or ecosystem level through traditional fieldwork and laboratory assays is impractical¹⁴.

This is where hyperspectral remote sensing may offer a powerful alternative. Hyperspectral data captures spectral information across a wide range of wavelengths and, through specific absorption features, enables the estimation of a series of plant traits^{15–17}. Therefore, hyperspectral satellite-borne remote sensing can provide an avenue for continuous monitoring of functional diversity across time and space¹⁸. Current and upcoming space-borne hyperspectral missions, such as EnMAP¹⁹, PRISMA²⁰, GaoFen-5²¹, CHIME²², and SBG²³, promise to deliver unprecedented volumes of

hyperspectral data, important steps towards a global system to track changes in plant traits and, by extension, functional diversity^{14,24,25}.

To harness the full potential of these hyperspectral datasets for functional diversity monitoring, it is essential to develop robust models capable of accurately predicting plant traits over time and across different ecosystems and vegetation types. Data-driven approaches, particularly machine learning, are powerful tools for retrieving trait information from hyperspectral imagery by learning complex relationships between spectral signatures and plant traits^{26,27}. Especially the combination of large data compilations and deep learning has shown great promise in improving the accuracy and scalability of trait prediction models^{17,28,29}.

Previous studies have managed to map functional diversity locally^{30–33}. However, so far, most of these surveys only cover a single point in time and ignore possible changes in functional diversity due to phenology. Other studies performed multi-temporal analyses of functional traits, but only for small areas, and did not specifically address functional diversity^{34,35}. A third group of studies focused on the link between spectral signals and functional diversity, but only through simulations^{36–38}. It is well known that values for plant functional traits change significantly throughout the vegetation period^{39,40} and also that these changes critically affect the retrieval of plant functional traits from spectral data⁴¹. It therefore remains unclear how representative functional diversity maps are across seasons.

¹Institute for Earth System Science and Remote Sensing, Leipzig University, Leipzig, Germany. ²Chair of Sensor-based Geoinformatics, University of Freiburg, Freiburg, Germany. ³Center for scalable data analytics and artificial intelligence (ScaDS.AI), Leipzig University - TU Dresden, Leipzig, Germany. ⁴Department of Biology - Ecoinformatics and Biodiversity, University of Aarhus, Aarhus, Denmark. ⁵Pioneer Center for Landscape Research in Sustainable Agricultural Futures (Land-CRAFT), Aarhus, Denmark. ⁶German Centre for Integrative Biodiversity Research (iDiv), Halle-Jena-Leipzig, Leipzig, Germany. ⁷Helmholtz-Centre for Environmental Research (UFZ), Leipzig, Germany. ✉e-mail: daniel.mederer@uni-leipzig.de

Here, we assess the seasonal variation in remotely sensed functional diversity and examine whether these patterns differ across biomes and along latitudinal gradients (see Fig. 1). We assembled a large global dataset of hyperspectral satellite images acquired by the EnMAP mission⁴², covering a two-year period from 2022 to 2024. For each scene of 30 km² with a 30 m × 30 m spatial resolution, we retrieved 20 essential plant functional traits through a deep learning model¹⁷. We calculated two functional diversity indices for the whole scene: Rao's Q, which measures trait dissimilarity, and functional richness, which captures the range of trait values. As our dataset provided broad spatial coverage rather than repeated observations at the same coordinates, these indices were compared based on the recording time of the scene and its geographical location to derive variations of functional diversity for five major biomes. While interpreting ecological drivers is beyond the scope of this study, our results demonstrate that functional diversity varies considerably across seasons and biomes, with metric-specific differences. These patterns suggest that single-time-point snapshots may not fully capture ecosystem functional diversity and hence impair assessments of ecosystem stability and functioning.

Results

Temporal variability among biomes

Across biomes, we found the data to vary substantially in time (Figs. 2 and 3). Overall, values of Rao's Q ranged from 1.54 to 6.85 for the entire time period, with higher values indicating higher functional diversity. Rainforests exhibited the lowest range of values (2.69–5.35), whereas the highest range for Rao's Q occurred in the Mediterranean ecosystems (2.20–6.85; Fig. 2). Savannas and Shrublands showed the most pronounced seasonal changes, followed by Temperate Grasslands and Mediterranean ecosystems. At the same time, Temperate Forests and Rainforests displayed the least variation. In Temperate Forests, subtle seasonal variations were observed for the Northern hemisphere, with Rao's Q values peaking during spring and autumn (Figs. 2 and 3). Temperate Grasslands also exhibited their maximum in Rao's Q values during spring and autumn in the Southern hemisphere (Figs. 2 and 3). For Savannas and Shrublands, pronounced seasonal patterns were detected, with higher Rao's Q values occurring between April and October in tropical zones and between March and November South of the tropics, corresponding to the wet season (Figs. 2 and 3). Rainforests showed a similar tendency, but exhibited no clear seasonal patterns in Rao's Q, which is consistent with the more stable climatic conditions in these ecosystems (Figs. 2 and 3). The Mediterranean ecosystems, Temperate Grasslands, as well as Savannas and Shrublands displayed substantial overall variation in Rao's Q throughout the vegetation period (Supplementary Fig. 1).

Differences between metrics

Functional richness generally displayed similar seasonal trends to those observed in Rao's Q (Supplementary Figs. 2–6), but interquartile ranges

were comparatively higher (Fig. 2, Supplementary Fig. 3). Overall functional richness values from convex hull ranged from 89.99 to 11798.05 for the entire time period, with higher values also indicating higher functional diversity. Temperate Grasslands displayed the lowest value range (89.99–6545.27), whereas the highest range of values for functional richness was found in Mediterranean ecosystems (457.14–11798.05). Functional richness patterns calculated by kernel density estimation hypervolume (KDE) showed high resemblance to those derived from convex hull (Supplementary Figs. 5 and 6) and exhibited a higher overall range of values (10203.09–305246.55).

To further quantify the differences between the two metrics, we calculated the means of monthly coefficients of variation (meanCVs). Rao's Q showed low to medium variability, with meanCVs ranging from 0.13 in Temperate Forests to 0.31 in Temperate Grasslands (Supplementary Fig. 7). In contrast, functional richness exhibited much higher variability, with meanCVs ranging from 0.33 in Temperate Forests to 0.96 in Temperate Grasslands (Supplementary Fig. 8).

Discussion

This study documents the pronounced temporal variation of remotely sensed functional diversity across five major biomes. Our results highlight the importance of incorporating temporal variation into functional diversity assessments. The observed temporal dynamics in functional diversity have implications for ecological research and biodiversity monitoring through Earth observation, as well as through conventional field surveys. It has to be noted, however, that the functional traits considered in our analysis are restricted to those that can be addressed with optical remote sensing data. This leads to a bias towards aboveground and specifically towards leaf traits of the dominant and sun-exposed canopy layer, whereas belowground traits, propagation or dispersal traits are not included. Also note that given the 30 m pixel size of EnMAP, we primarily address functional diversity of plant communities. We can therefore not make statements about all possible aspects of functional diversity.

Temporal variation in functional diversity differs extensively across biomes, underscoring the influence of ecological and climatic contexts. Rainforests, for example, exhibit minimal seasonal variation in Rao's Q and functional richness, reflecting the more stable climatic conditions of these ecosystems. In contrast, Savannas and Shrublands show stronger seasonal changes that accompany the prevailing wet-dry cycles. One caveat of these results is data scarcity in wet seasons due to fundamental limitations of optical remote sensing concerning high cloud cover¹⁴. At the same time, Mediterranean ecosystems and Temperate Grasslands exhibit substantial seasonal variation, where functional diversity peaks mainly during the spring and autumn months. These peaks were also observed for Temperate Forests in a less pronounced form, suggesting that the times of budburst and leaf senescence lead to high levels of remotely sensed functional diversity. In general, all these findings align with previous work indicating the strong

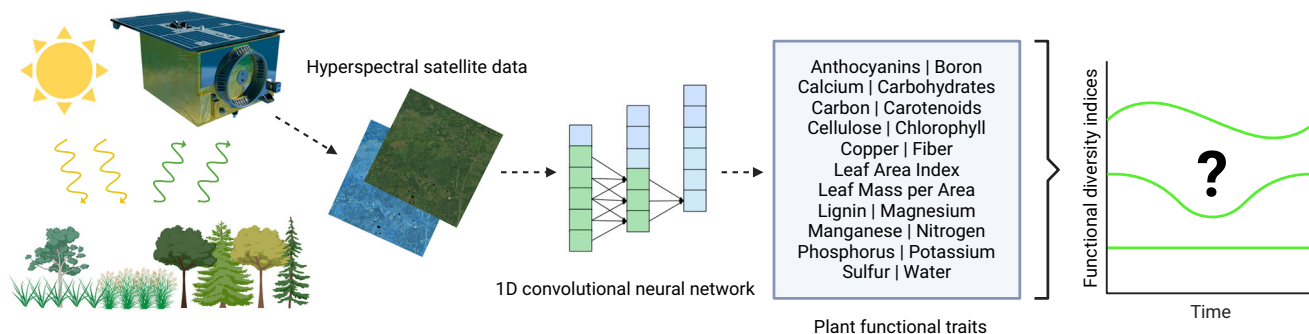


Fig. 1 | General workflow of the multi-seasonal functional diversity analysis⁵⁸. Hyperspectral data of the EnMAP satellite mission¹⁹ is fed into a one-dimensional (1D) convolutional neural network¹⁷, which predicts 20 different plant functional

traits per scene. These traits are then used to calculate functional diversity indices and analyze their changes over time.

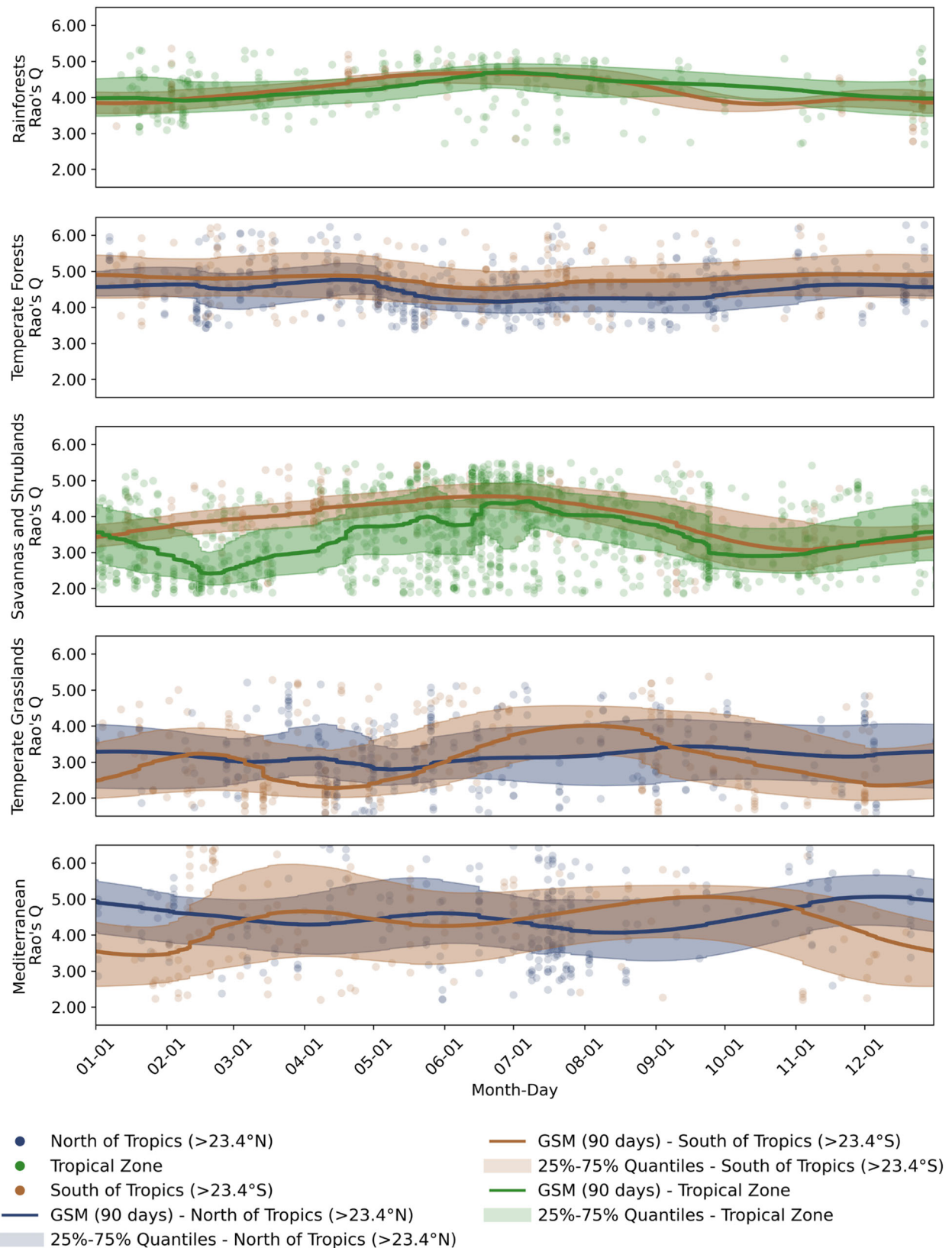


Fig. 2 | Scatter plots of Rao's Q (trait dissimilarity) values for the five different biomes. Values North of the tropics were excluded for Rainforests as well as Savannas and Shrublands due to sparse data. Image acquisition dates are merged

across years. A Gaussian smoothed median (GSM) with a moving window of 90 days is shown for each latitude group of each plot, along with colored bars representing the range from 25% to 75% quantiles.

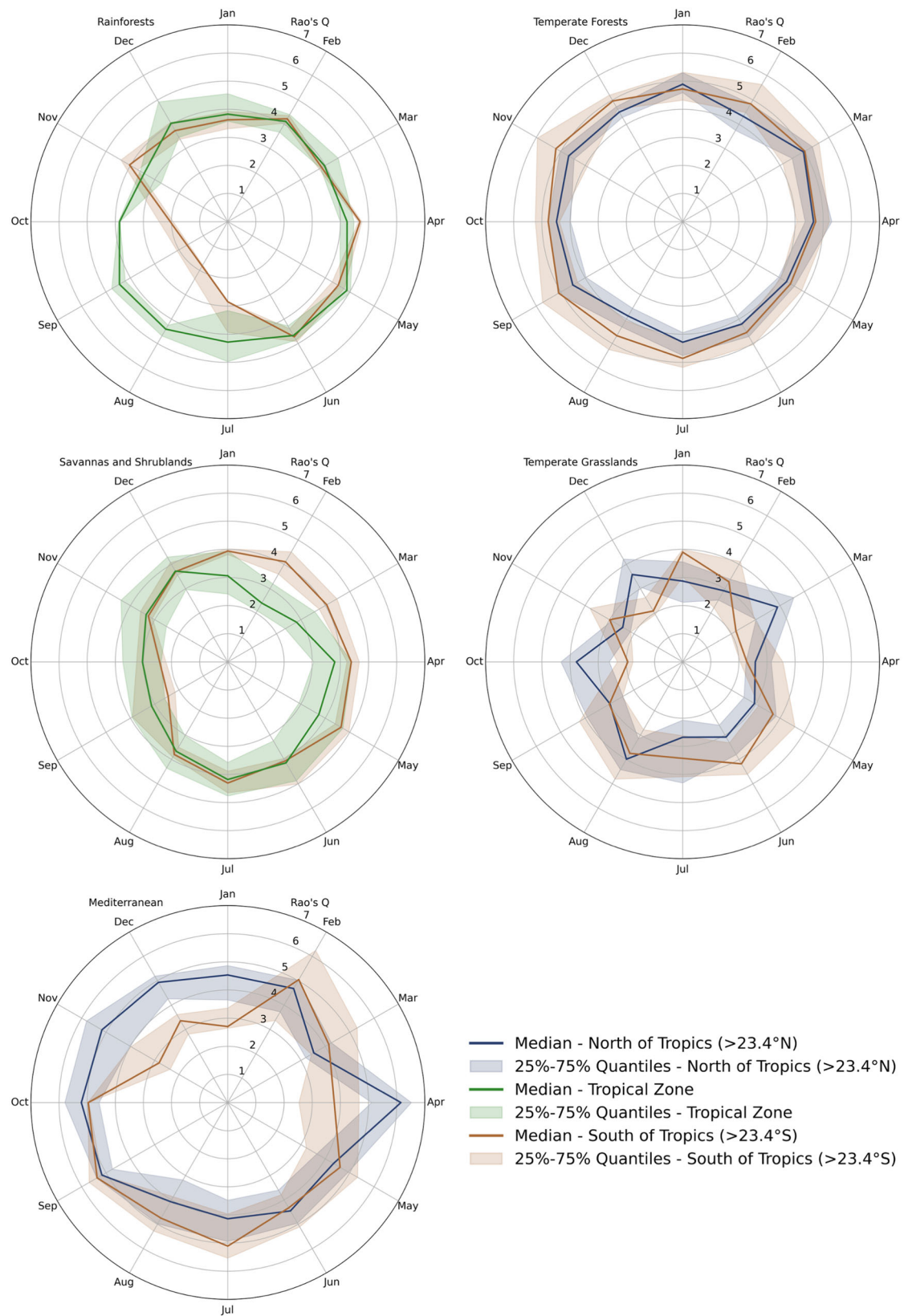


Fig. 3 | Polar plots of Rao's Q (trait dissimilarity) values for the five different biomes. Values North of the tropics are not shown for Rainforests and Savannas and Shrublands due to sparse data. Image acquisition dates are merged across years. The

monthly median is shown for each latitude group of each plot, along with colored bars representing a range from 25% to 75% monthly quantiles.

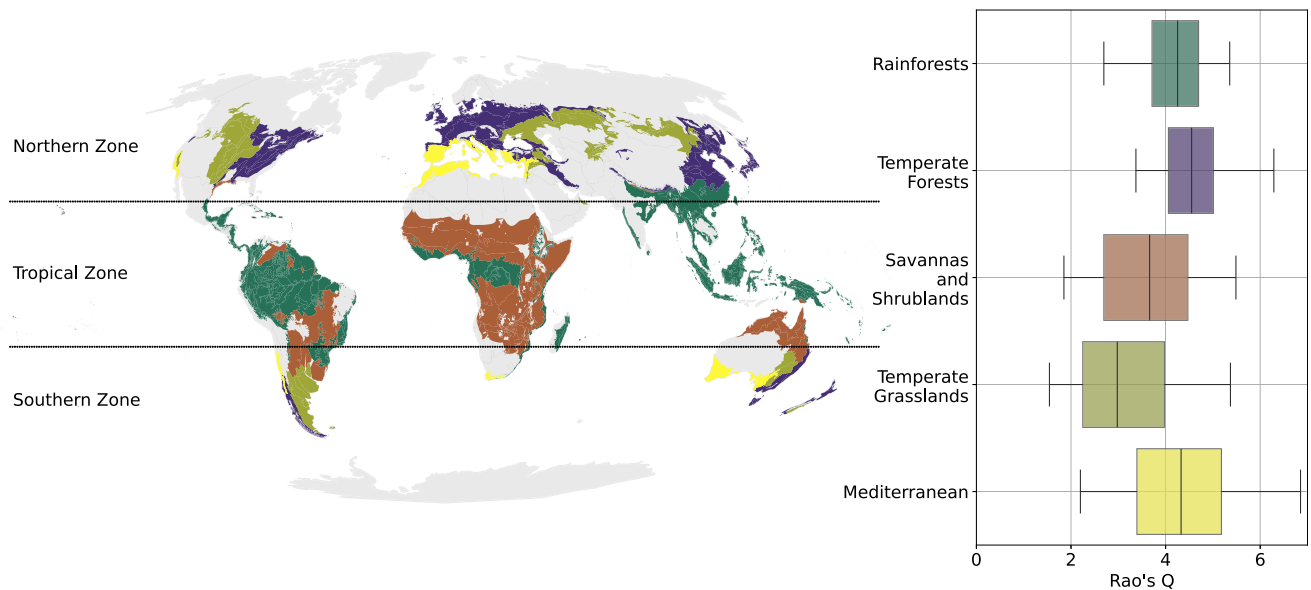


Fig. 4 | Location of the five biomes in our study using the Mollweide projection. Dotted black lines separate the three latitude groups. Boxplots show the monthly Rao's Q (trait dissimilarity) medians for all biomes without differentiation by

latitude. The boxes show the interquartile range (IQR) and the median of medians, while the whiskers extend to the smallest and largest median values within 1.5 times the IQR.

phenological and environmental controls on plant traits^{39,40,43,44}, which evidently apply also to functional diversity (compare Durán et al.⁴⁵). The observed seasonal trends emphasize that temporal snapshots may not reveal the full picture of functional diversity (see Guimarães-Steinicke et al.⁴⁶). This also highlights that comparing functional diversity estimated in different seasons may be misleading. Moreover, comparing functional diversity estimates across regions, which may not have a synchronous seasonal behavior, may also be misleading. Uncertainties will be particularly severe in ecosystems with high overall value ranges for diversity estimates, which in our study were found for Temperate Grasslands, Savannas and Shrublands and the Mediterranean (Supplementary Fig. 1). It should be noted, however, that Supplementary Figs. 1, 2 and Fig. 4 do not show which biomes are the most functionally diverse overall, but only provide a comparison at a resolution of $30 \text{ m} \times 30 \text{ m}$ and a spatial extent of 30 km^2 . This means that we do not observe functional diversity at the species level, but quantify diversity gradients of plant communities on a landscape scale. This inevitably leads to lower overall diversity, but it allows us to observe biodiversity patterns at the biome level. Since plant sizes and compositional patterns differ widely between life forms and ecosystems, more comprehensive and reliable comparisons between biomes would have to take the effects of scale and multiple spatial resolutions into account^{36,37}.

The choice of metric for functional diversity also influences the observed temporal patterns. Rao's Q shows relatively low variation, while functional richness exhibits higher variation, particularly during the seasons with the highest values (Supplementary Figs. 3, 4). This can be explained by the dependency of functional richness on species numbers (Villéger et al., 2008), which have a less prominent influence on Rao's Q. Functional richness also exhibits coefficients of variation that are up to three times higher than those of Rao's Q (Supplementary Figs. 7, 8). In general, these findings highlight the importance of selecting functional diversity metrics. Rao's Q and functional richness are different facets of functional diversity, and while Rao's Q is more frequently used, the choice depends on the assessment's focus. Thus, combining multiple metrics can provide a more nuanced understanding of functional diversity dynamics³⁷.

The possible extent of uncertainty in our results depends on the accumulated uncertainties of the model's trait predictions. Here, the robustness of the model itself remains a possible caveat since we cannot assess the temporal variation of the model in detail due to a general lack of validation data. Assembling a benchmark dataset of plant trait

observations at a global scale, with sufficiently large plots and co-located hyperspectral data, is a long-standing goal in vegetation remote sensing - one that will require sustained, coordinated efforts across the research community^{14,18}. However, we assessed the trait predictions in our study over time (Supplementary Figs. 9–28), particularly for two of the seasonally most affected traits, Chlorophyll and LAI (Supplementary Figs. 29, 30), and found consistent seasonal patterns in line with the expectations. We also know that the model of Cherif et al.¹⁷ was trained and successfully evaluated on 42 datasets of different biomes with large temporal variation. According to their results and our own assessments of temporal variation, we therefore assume that the model predictions are robust. Regarding uncertainty in the functional diversity metrics, we are aware that functional richness calculated via convex hull volume can be sensitive to outliers, as extreme trait combinations disproportionately influence the geometry of the hull. To address this, we decided to include KDE as an alternative method for calculating functional richness. KDE-based methods are generally less sensitive to outliers, as they weigh the density of trait distributions rather than relying solely on the outermost points. KDE results show high resemblance with the ones obtained from convex hull, which indicates the robustness of functional richness estimates (Supplementary Figs. 5, 6). Rao's Q has low sensitivity to outliers, as it is based on pairwise trait dissimilarities across the trait space, rather than being dependent on the outer envelope. It integrates over all distances and does not emphasize extremes. As such, Rao's Q is often considered a more stable metric when dealing with continuous trait distributions^{47,48}. Both Rao's Q and convex hull are parameter-free and deterministic once the trait distance matrix is defined. There is no inherent stochasticity or calibration involved in their calculation, and uncertainty arises primarily from input variability rather than from the metric formulation itself. Another uncertainty factor is any misclassification in the European Space Agency (ESA) WorldCover product that we used to mask out anthropogenic land cover types in the EnMAP scenes. Examples would be agricultural areas misclassified as Temperate Grasslands or tree plantations misclassified as Rainforests. However, the ESA WorldCover is currently the most accurate product available⁴⁹. It has a $10 \text{ m} \times 10 \text{ m}$ spatial resolution, which means that the extent of misclassification in our scenes with $30 \text{ m} \times 30 \text{ m}$ pixels was considered to be minimal. Lastly, at current processing levels, EnMAP products do not include Bidirectional Reflectance Distribution Function (BRDF)

correction, i.e. the removal of effects resulting from different illumination and observation angles. The model in our study was trained on airborne data with varying levels of BRDF and illumination effects. BRDF effects primarily result in changes in the magnitude of reflectance rather than the shape. Our method (Convolutional Neural Networks) is primarily dependent on shape-related features and was augmented during training with systematic shifts in reflectance magnitudes¹⁷. It should therefore be robust to satellite-level BRDF.

Our study underscores the value of hyperspectral remote sensing for tracking temporal dynamics in functional diversity. While remote sensing primarily reveals the functional diversity of dominant plants and may miss the diversity beneath the upper canopy, it remains a powerful tool due to its standardized, repeated, and large-scale observations¹⁴. The ability to retrieve plant traits across time and space provides unprecedented opportunities for ecosystem monitoring, particularly in remote or inaccessible regions. However, we also encountered challenges, including data gaps in tropical rainforests and savanna regions due to cloud cover and limited satellite scene availability. It should also be noted that we excluded boreal forests and the tundra biome after data collection due to severe data scarcity. These gaps necessarily limit the generalizability of our findings. Nevertheless, the seasonal changes observed in temperate biomes, especially since they correlate with leaf phenology, imply that boreal forests and the tundra biome should also exhibit pronounced seasonality effects. Additionally, sampling bias likely plays a role in our results due to EnMAP's snapshot-on-demand coverage that lacks spatiotemporal continuity, particularly in the relatively stable pattern of functional diversity in Temperate Forests (Fig. 2, Supplementary Fig. 3). This biome includes both deciduous and mixed forests, and values during winter are more likely to come from mixed forests dominated by conifers than from deciduous ones. Addressing these limitations through enhanced satellite coverage and improved cloud-masking algorithms will be essential for achieving global functional diversity monitoring. More frequently available Landsat or Sentinel data with a few multispectral bands cannot fill the data gap since rich hyperspectral data are crucial to retrieve the analyzed key plant traits, including leaf water and nitrogen content¹⁸. Therefore, future hyperspectral missions such as CHIME²² and SBG²³ promise a more comprehensive spatiotemporal picture across all biomes. Above all, there is an urgent need for more dense temporal coverage of hyperspectral acquisitions. Additionally, the sensitivity of trait retrieval to seasonal changes⁴¹ reinforces the need for robust, temporally adaptive models. The opportunities provided by deep learning-based trait estimation are especially promising in this context, as large, curated datasets¹⁷ now enable the inference of a wider range of traits essential for describing functional diversity. As more researchers share data, including those of underrepresented traits and regions (see Mederer et al.⁵⁰), the capacity to monitor functional diversity will continue to grow.

Conclusion

This study underscores the importance of integrating temporal dynamics into functional diversity assessments. Our findings provide evidence that functional diversity exhibits substantial variation across seasons, biomes, and diversity metrics. Seasonal trends revealed in our analysis suggest that single temporal snapshots fail to capture the full complexity of functional diversity, which underscores the risk of misinterpretation when comparing estimates from different time points. Similarly, cross-regional comparisons of functional diversity may yield misleading conclusions if they do not account for asynchronous seasonal patterns among regions. These insights call for a shift from static to multitemporal functional diversity monitoring, leveraging the growing availability of hyperspectral satellite data. However, using hyperspectral data does not automatically provide a comprehensive solution (cf. Jetz et al.¹⁴). The choice of functional diversity metric depends on the specific goals of a study, as different metrics emphasize different aspects of diversity. Each has its limitations regarding trait selection, spatial resolution and temporal coverage. At the same time, more efforts are needed to promote data sharing across research communities, which will enable the inclusion of underrepresented regions in global analyses. By fostering collaborative initiatives and leveraging multitemporal monitoring, we can bridge critical data gaps and enhance the accuracy of functional diversity assessments. This will make it possible to unlock the full potential of functional diversity assessments to inform biodiversity science and sustainable ecosystem management on a global scale.

Methods

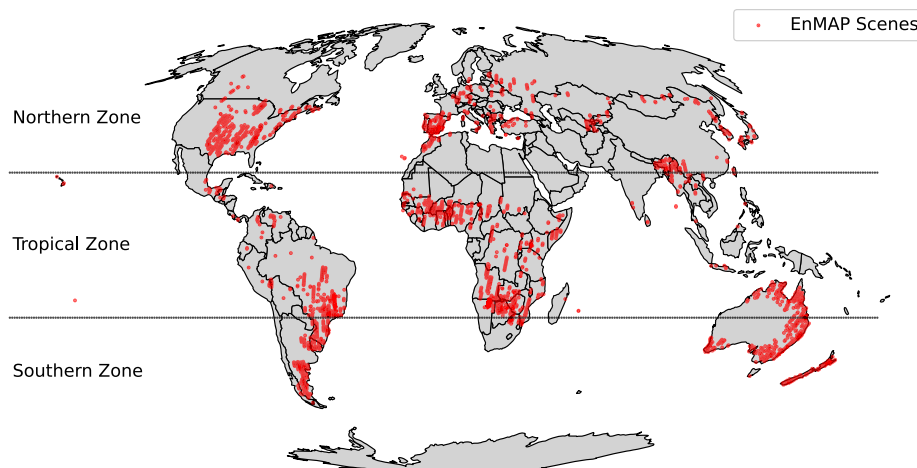
Dataset collection

We acquired 4157 EnMAP scenes from the corresponding website⁵¹. Their global distribution is shown in Fig. 5. The data were preprocessed to Level-2A data in GeoTIFF format with combined land and water correction and no ozone correction. We selected all available EnMAP scenes at the time (15.09.2024) that met the following criteria:

- located in one of the five biomes we studied (Fig. 4)
- covering mostly natural vegetation; national parks and protected areas where prioritized, in doubt we cross-checked with the ESA World-Cover dataset⁵²
- cloud cover below 50%
- no dispersed cloud cover

Our study includes five biomes of the World Wildlife Fund Terrestrial Ecoregions Of The World dataset⁵³. These were (with abbreviations in brackets): Tropical and subtropical moist broadleaf forests (Rainforests), Temperate broadleaf and mixed forests (Temperate Forests), Tropical and subtropical grasslands, savannas and shrublands (Savannas and Shrublands), Temperate grasslands, savannas and shrublands (Temperate Grasslands) and Mediterranean Forests, woodlands and scrubs (Mediterranean).

Fig. 5 | Distribution of EnMAP satellite scenes in our dataset using the Mollweide projection. One red dot represents one scene, while dotted black lines separate the three latitude groups.



Data coverage

Rainforests as well as Savannas and Shrublands North of the tropics were excluded due to insufficient coverage, while areas South of the tropics had limited representation, reflecting their latitude-dependent distribution. Across the tropics, high cloud cover and relatively few requested satellite scenes posed challenges (Figs. 4, 5). Nevertheless, the vast natural expanses of these regions provided sufficient data, with 538 scenes available for analysis. Savannas and Shrublands exhibited the highest data coverage (1693 scenes), primarily due to the extensive areas in Africa and Australia that combine high scene requests with low levels of anthropogenic disturbance. Temperate Forests (806 scenes) and Temperate Grasslands (645 scenes) were well covered despite extensive anthropogenic land cover changes, particularly from agricultural expansion. Mediterranean ecosystems, while represented by the smallest total number of scenes (475), benefited from very high coverage relative to their limited geographic extent.

Model implementation

We employed a pre-trained one-dimensional CNN model for retrieving plant traits from spectral data, provided by Cherif et al.¹⁷ via GitHub⁵⁴. The architecture, adapted from EfficientNet-B0⁵⁵ for one-dimensional input, incorporates depthwise separable convolutions and network scaling techniques. The model predicts 20 plant functional traits at once and was trained on a global collection of 42 different datasets. This collection includes hyperspectral data obtained from various remote sensing platforms and sensors (e.g. AVIRIS, HyMap, HySpex, NEON Airborne Observation Platform AOP). Despite having different spectral properties, they cover a comparable wavelength range of the solar electromagnetic spectrum (see Table A.1 in Cherif et al.¹⁷). Measurements were unified across the full range of 400–2500 nm in 1 nm steps by applying a forward and backward linear interpolation¹⁷. The model transferability was evaluated with a block cross-validation across 42 independent datasets. Evaluation results were then averaged for the final R-squared (R^2) and normalized Root Mean Squared Error (nRMSE) values, which ranged from 0.10 to 0.69 for R^2 and 19.92 to 10.65 for nRMSE. Notably, many of the most important plant traits such as chlorophyll (0.51 R^2 , 16.92 nRMSE), nitrogen (0.42 R^2 , 14.28 nRMSE) and leaf mass per area (0.69 R^2 , 10.65 nRMSE) were predicted with high accuracy, therefore showing that the model is able to predict these traits reliably across different biomes and ecosystems. All model settings were kept identical to those in Cherif et al.'s original work and were implemented in Python.

Preprocessing

We used the five masks provided by EnMAP (cloud, cirrus, cloud-shadow, haze, snow) to eliminate non-vegetation surface elements in the scene. To deal with mask artifacts, a binary dilation buffer with a radius of 40 pixels was chosen after testing different values. Topography correction using a digital elevation model has already been applied by the EnMAP pre-processing pipeline for L2A data. All masks were merged and then applied on the scene. Furthermore, since EnMAP scenes have a rhomboid shape with padding of no-data values around them, each scene was cropped to an axis-parallel rectangle using the outer coordinates of the scene. Next, we masked all man-made surface elements and water (built-up area, croplands, permanent water and snow/ice) identified in the ESA WorldCover V2 2021 dataset³².

Prediction and evaluation

We drew a random sample of $n = 5000$ pixels from the remaining areas comprising natural and semi-natural, sunlit, vegetated pixels. On these pixels, we applied the trait model, predicting 20 plant functional trait values, resulting in a total of 100,000 trait values per scene. A heatmap with mean trait values and ranges per biome is available in the supplementary material (Supplementary Fig. 31). The values were then standardized to a mean of 0 and a standard deviation of 1 before being subject to a Principal Component Analysis (PCA). Standardization and PCA were first done globally for all scenes at once, and then the component loadings were used for the

individual scenes (Supplementary Fig. 32). We created a PCA biplot to visualize how the traits influence the main two axes (Supplementary Fig. 33). Over 90% of the variance is explained by the first five components of the PCA (Supplementary Fig. 34), therefore we chose these as the basis for calculating both the Rao's Q and functional richness value for each scene. Both metrics were chosen because they are widely used by the community and measure different aspects of functional diversity.

Rao's Q measures diversity as trait dissimilarity by considering the weighted average of all pairwise differences between values, where the weights are based on the relative proportions of each data point following Eq. (1).

$$Q = \sum_{i=1}^n \sum_{j=1}^n p_i p_j d(x_i, x_j) \quad (1)$$

Where p_i and p_j are the relative proportions associated with data points x_i and x_j and $d(x_i, x_j)$ is the difference between x_i and x_j . Functional richness measures diversity as the range of plant functional trait values and was calculated in two ways. First, as the volume of the convex hull in the 5-dimensional PCA-space. For this we used the convex hull function from SciPy in python⁵⁶. Second, functional richness was calculated as the kernel density estimation hypervolume (KDE) of the 5-dimensional PCA-space, as this method might be less prone to data outliers. Here we used the KernelDensity function from scikit-learn in python⁵⁷. Bandwidth was set to 0.5 after applying GridSearchCV from scikit-learn to ten scenes from each of the five biomes. The threshold was set to the 95% quantile and the generated samples to 50,000. Values below 5% and above the 95% quantiles for both metrics were removed to prevent distortions from extreme outliers.

Code availability

The complete code for the model can be found here: <https://github.com/echerif18/multiTraitPredictions>.

Data availability

All predictions and auxiliary data for the global PCA can be downloaded here: <https://doi.org/10.5281/zenodo.15089926>. EnMAP scenes are freely available on this website: https://geoservice.dlr.de/eoc/ogc/stac/v1/collections/ENMAP_HSI_L2A.

Received: 24 April 2025; Accepted: 30 July 2025;

Published online: 06 October 2025

References

1. Díaz, S. et al. The IPBES Conceptual Framework—connecting nature and people. *Curr. Opin. Environ. Sustain.* **14**, 1–16 (2015).
2. Bongers, F. J. et al. Functional diversity effects on productivity increase with age in a forest biodiversity experiment. *Nat. Ecol. Evol.* **5**, 1594–1603 (2021).
3. Tilman, D. et al. The influence of functional diversity and composition on ecosystem processes. *Science* **277**, 1300–1302 (1997).
4. Van Der Plas, F. Biodiversity and ecosystem functioning in naturally assembled communities. *Biol. Rev.* **94**, 1220–1245 (2019).
5. Jochum, M. et al. The results of biodiversity–ecosystem functioning experiments are realistic. *Nat. Ecol. Evol.* **4**, 1485–1494 (2020).
6. de Bello, F. et al. Functional trait effects on ecosystem stability: assembling the jigsaw puzzle. *Trends Ecol. Evol.* **36**, 822–836 (2021).
7. Funk, J. L. et al. Revisiting the Holy Grail: using plant functional traits to understand ecological processes. *Biol. Rev.* **92**, 1156–1173 (2017).
8. Lavorel, S. & Garnier, E. Predicting changes in community composition and ecosystem functioning from plant traits: revisiting the Holy Grail. *Plant response and effect groups. Funct. Ecol.* **16**, 545–556 (2002).
9. Mason, N. W., Mouillot, D., Lee, W. G. & Wilson, J. B. Functional richness, functional evenness and functional divergence: the primary components of functional diversity. *Oikos* **111**, 112–118 (2005).

10. Villéger, S., Mason, N. W. & Mouillot, D. New multidimensional functional diversity indices for a multifaceted framework in functional ecology. *Ecology* **89**, 2290–2301 (2008).
11. Laliberté, E. & Legendre, P. A distance-based framework for measuring functional diversity from multiple traits. *Ecology* **91**, 299–305 (2010).
12. Maire, V. et al. Global effects of soil and climate on leaf photosynthetic traits and rates. *Glob. Ecol. Biogeogr.* **24**, 706–717 (2015).
13. Joswig, J. S. et al. Climatic and soil factors explain the two-dimensional spectrum of global plant trait variation. *Nat. Ecol. Evol.* **6**, 36–50 (2022).
14. Jetz, W. et al. Monitoring plant functional diversity from space. *Nat. Plants* **2**, 1–5 (2016).
15. Asner, G. P. & Martin, R. E. Airborne spectranomics: mapping canopy chemical and taxonomic diversity in tropical forests. *Front. Ecol. Environ.* **7**, 269–276 (2009).
16. Wang, Z. et al. Foliar functional traits from imaging spectroscopy across biomes in eastern North America. *N. Phytol.* **228**, 494–511 (2020).
17. Cherif, E. et al. From spectra to plant functional traits: Transferable multi-trait models from heterogeneous and sparse data. *Remote Sens. Environ.* **292**, 113580 (2023).
18. *Remote Sensing of Plant Biodiversity* (Springer International Publishing, 2020). <https://doi.org/10.1007/978-3-030-33157-3>.
19. Guanter, L. et al. The EnMAP spaceborne imaging spectroscopy mission for earth observation. *Remote Sens.* **7**, 8830–8857 (2015).
20. Loizzo, R. et al. PRISMA: the Italian hyperspectral mission. In *IGARSS 2018 - 2018 IEEE International Geoscience and Remote Sensing Symposium*, 175–178 (IEEE, 2018).
21. Liu, Y.-N. et al. The advanced hyperspectral imager: aboard China's gaoFen-5 satellite. *IEEE Geosci. Remote Sens. Mag.* **7**, 23–32 (2019).
22. Nieke, J. et al. The copernicus hyperspectral imaging mission for the environment (CHIME): an overview of its mission, system and planning status. *Sens. Syst. Gener. Satell.* **XXVII** **12729**, 21–40 (2023).
23. Cawse-Nicholson, K. et al. NASA's surface biology and geology designated observable: a perspective on surface imaging algorithms. *Remote Sens. Environ.* **257**, 112349 (2021).
24. Sciences, N. A. et al. *Thriving on Our Changing Planet: A Decadal Strategy for Earth Observation from Space* (National Academies Press, 2019).
25. Proença, V. et al. Global biodiversity monitoring: from data sources to essential biodiversity variables. *Biol. Conserv.* **213**, 256–263 (2017).
26. Verrelst, J. et al. Optical remote sensing and the retrieval of terrestrial vegetation bio-geophysical properties – A review. *ISPRS J. Photogramm. Remote Sens.* **108**, 273–290 (2015).
27. Verrelst, J. et al. Quantifying vegetation biophysical variables from imaging spectroscopy data: a review on retrieval methods. *Surv. Geophys.* **40**, 589–629 (2019).
28. Yuan, Q. et al. Deep learning in environmental remote sensing: achievements and challenges. *Remote Sens. Environ.* **241**, 111716 (2020).
29. Kattenborn, T., Leitloff, J., Schiefer, F. & Hinz, S. Review on Convolutional Neural Networks (CNN) in vegetation remote sensing. *ISPRS J. Photogramm. Remote Sens.* **173**, 24–49 (2021).
30. Schneider, F. D. et al. Mapping functional diversity from remotely sensed morphological and physiological forest traits. *Nat. Commun.* **8**, 1441 (2017).
31. Schweiger, A. K. et al. Plant spectral diversity integrates functional and phylogenetic components of biodiversity and predicts ecosystem function. *Nat. Ecol. Evol.* **2**, 976–982 (2018).
32. Zheng, Z. et al. Mapping functional diversity using individual tree-based morphological and physiological traits in a subtropical forest. *Remote Sens. Environ.* **252**, 112170 (2021).
33. Cavender-Bares, J. et al. Remotely detected aboveground plant function predicts belowground processes in two prairie diversity experiments. *Ecol. Monogr.* **92**, e01488 (2022).
34. Feilhauer, H., Somers, B. & Van Der Linden, S. Optical trait indicators for remote sensing of plant species composition: Predictive power and seasonal variability. *Ecol. Indic.* **73**, 825–833 (2017).
35. Chlus, A. & Townsend, P. A. Characterizing seasonal variation in foliar biochemistry with airborne imaging spectroscopy. *Remote Sens. Environ.* **275**, 113023 (2022).
36. Ludwig, A., Doktor, D. & Feilhauer, H. Is spectral pixel-to-pixel variation a reliable indicator of grassland biodiversity? A systematic assessment of the spectral variation hypothesis using spatial simulation experiments. *Remote Sens. Environ.* **302**, 113988 (2024).
37. Pacheco-Labrador, J. et al. Challenging the link between functional and spectral diversity with radiative transfer modeling and data. *Remote Sens. Environ.* **280**, 113170 (2022).
38. Pacheco-Labrador, J. et al. A generalizable normalization for assessing plant functional diversity metrics across scales from remote sensing. *Methods Ecol. Evol.* **14**, 2123–2136 (2023).
39. McKown, A. D., Guy, R. D., Azam, M. S., Drewes, E. C. & Quamme, L. K. Seasonality and phenology alter functional leaf traits. *Oecologia* **172**, 653–665 (2013).
40. Fajardo, A. & Siefert, A. Phenological variation of leaf functional traits within species. *Oecologia* **180**, 951–959 (2016).
41. Schiefer, F., Schmidlein, S. & Kattenborn, T. The retrieval of plant functional traits from canopy spectra through RTM-inversions and statistical models are both critically affected by plant phenology. *Ecol. Indic.* **121**, 107062 (2021).
42. Chabrillat, S. et al. The EnMAP spaceborne imaging spectroscopy mission: initial scientific results two years after launch. *Remote Sens. Environ.* **315**, 114379 (2024).
43. Noda, H. M. et al. Phenology of leaf morphological, photosynthetic, and nitrogen use characteristics of canopy trees in a cool-temperate deciduous broadleaf forest at Takayama, central Japan. *Ecol. Res.* **30**, 247–266 (2015).
44. Yang, X. et al. Seasonal variability of multiple leaf traits captured by leaf spectroscopy at two temperate deciduous forests. *Remote Sens. Environ.* **179**, 1–12 (2016).
45. Durán, S. M. et al. Informing trait-based ecology by assessing remotely sensed functional diversity across a broad tropical temperature gradient. *Sci. Adv.* **5**, eaaw8114 (2019).
46. Guimarães-Steinicke, C. et al. Terrestrial laser scanning reveals temporal changes in biodiversity mechanisms driving grassland productivity. In *Advances in Ecological Research* vol. 61 133–161 (Elsevier, 2019).
47. Botta-Dukát, Z. Rao's quadratic entropy as a measure of functional diversity based on multiple traits. *J. Vegetation Sci.* **16**, 533–540 (2005).
48. Ricotta, C. & Moretti, M. CWM and Rao's quadratic diversity: a unified framework for functional ecology. *Oecologia* **167**, 181–188 (2011).
49. Xu, P. et al. Comparative validation of recent 10 m-resolution global land cover maps. *Remote Sens. Environ.* **311**, 114316 (2024).
50. Mederer, D. et al. Plant trait retrieval from hyperspectral data: collective efforts in scientific data curation outperform simulated data derived from the PROSAIL model. *ISPRS Open J. Photogramm. Remote Sens.* **15**, 100080 (2025).
51. EnMAP Instrument Planning. <https://planning.enmap.org/> (2021).
52. WorldCover Viewer. https://viewer.esa-worldcover.org/worldcover/?language=en&bbox=-351.56249999999994,-70.55417853776078,180.00000000000003,84.28470439392032&overlay=false&bgLayer=OSM&date=2025-03-17&layer=WORLDCOVER_2021_MAP (2021).
53. Olson, D. M. et al. Terrestrial ecoregions of the world: a new map of life on Earth: a new global map of terrestrial ecoregions provides an innovative tool for conserving biodiversity. *BioScience* **51**, 933–938 (2001).
54. EyaCherif. <https://github.com/echerif18/multiTraitPredictions> (2024).

55. Tan, M. & Le, Q. Efficientnet: rethinking model scaling for convolutional neural networks. In *International conference on machine learning* 6105–6114 (PMLR, 2019).
56. SciPy. GitHub <https://github.com/scipy> (2025).
57. scikit-learn. GitHub <https://github.com/scikit-learn/scikit-learn> (2025).
58. Mederer, D. Created in BioRender <https://BioRender.com/ckixtsz> (2025).

Acknowledgements

We thank Marvin Müller for his help in preprocessing the EnMAP scenes and all data owners for sharing the data either by request (in particular the consortium of the EU BiodivERsA project DIARS) or through the public Ecological Spectral Information System (EcoSIS), Data Publisher for Earth & Environmental Science (PANGAEA) and DRYAD platforms. DM and HF acknowledge support for this work from the Federal Ministry for Economic Affairs and Climate Action (BMWK) and the German Aerospace Center (DLR) through the project AIResVeg (grant 50EE2203A). H.F. and E.C. acknowledge the financial support by the Federal Ministry of Education and Research of Germany (BMBF) and by the Sächsische Staatsministerium für Wissenschaft, Kultur und Tourismus in the program Center of Excellence for AI-research “Center for Scalable Data Analytics and Artificial Intelligence Dresden/Leipzig”, project identification number: ScaDS.AI. T.K. acknowledges funding by the German Research Foundation (DFG) for the project PANOPS (grant-no. 504978936). FDS acknowledges funding by the Pioneer Center for Landscape Research in Sustainable Agricultural Futures (Land-CRAFT), DNRf grant number P2.

Author contributions

Daniel Mederer: Writing – original draft, Visualization, Methodology, Formal analysis, Data curation, Conceptualization. Teja Kattenborn: Writing – original draft, Supervision, Conceptualization. Eya Cherif: Writing – review & editing, Data curation. Claudia Guimaraes-Steinicke: Writing – review & editing. Julia S. Joswig: Writing – review & editing. Fabian D. Schneider: Writing – review & editing. Hannes Feilhauer: Writing – original draft, Supervision, Data curation, Conceptualization.

Funding

Open Access funding enabled and organized by Projekt DEAL.

Competing interests

The authors declare no competing interests.

Additional information

Supplementary information The online version contains supplementary material available at <https://doi.org/10.1038/s43247-025-02646-x>.

Correspondence and requests for materials should be addressed to Daniel Mederer.

Peer review information *Communications Earth and Environment* thanks Anning Zhang, Baodong Xu and the other, anonymous, reviewer(s) for their contribution to the peer review of this work. Peer review was single-anonymous OR Peer review was double-anonymous. Primary Handling Editors: Guiyao Zhou and Mengjie Wang. [A peer review file is available].

Reprints and permissions information is available at <http://www.nature.com/reprints>

Publisher's note Springer Nature remains neutral with regard to jurisdictional claims in published maps and institutional affiliations.

Open Access This article is licensed under a Creative Commons Attribution 4.0 International License, which permits use, sharing, adaptation, distribution and reproduction in any medium or format, as long as you give appropriate credit to the original author(s) and the source, provide a link to the Creative Commons licence, and indicate if changes were made. The images or other third party material in this article are included in the article's Creative Commons licence, unless indicated otherwise in a credit line to the material. If material is not included in the article's Creative Commons licence and your intended use is not permitted by statutory regulation or exceeds the permitted use, you will need to obtain permission directly from the copyright holder. To view a copy of this licence, visit <http://creativecommons.org/licenses/by/4.0/>.

© The Author(s) 2025